PCCP

Accepted Manuscript

ROYAL SOCIETY OF CHEMISTRY

www.rsc.org/pccp

Heavy Snow: IR spectroscopy of isotope mixed crystalline water ice

Authors

Andy Wong[1], Liang Shi[2], Rebecca Auchettl[3], Don McNaughton[1], Dominique Appadoo[4], Evan G. Robertson[3*].

1. School of Chemistry, Monash University, Wellington Road, Clayton, Victoria, 3800, Australia.

2. Theoretical Chemistry Institute and Department of Chemistry, University of Wisconsin, Madison, Wisconsin 53706, USA.

3. Department of Chemistry and Physics, La Trobe Institute for Molecular Science, La Trobe University, Victoria, 3086, Australia.

4. Australian Synchrotron, 800 Blackburn Road, Clayton, Victoria, 3148, Australia.

* Corresponding author: e.robertson@latrobe.edu.au

Abstract

Mid-infrared spectra have been measured for crystalline water ice aerosols of widely varied H/D isotopic composition. Particles with diameters ranging from 10 – 200 nm were generated via rapid collisional cooling with a cold buffer gas over a range of temperatures from 7 – 200 K. In near isotopically pure ices, the ν_L band position is slightly red-shifted with increasing temperature whilst in the ν_2 region apparently anomalous shifts in peak maxima are explained by the contribution of broad $2\,\nu_L$ band of H_2O and $3\,\nu_L$ band of D_2O together with ν_2 intensity that is particularly weak in low temperature crystalline ice. The hydrogen bonded OH (or OD) oscillator bands of near pure H_2O (or D_2O) ices are blue-shifted with temperature, with a gradient very similar to that of the corresponding band in isotope diluted samples, HOD in D_2O (or H_2O). It implies that this observed temperature trend is predominantly due to the intrinsic change in local hydride stretch potential energy, rather than to changes in intermolecular coupling. However, it is also observed that the narrow hydride stretch bands of isotope diluted sample rapidly develops phonon structure as the oscillator concentration increases, evidence of strong intermolecular coupling and a high degree of delocalisation. Anomalous blue-shifts in the OD stretch profile as D_2O concentration grows is attributable to Fermi resonance with $2\,\nu_2$ of D_2O, in much closer proximity than the corresponding H_2O levels. Theoretical results from a mixed quantum/classical approach are used to validate these findings in the hydride stretching region. Theory qualitatively reproduces the experimental trends as a function of temperature and isotopic variance.

Introduction

Water is a remarkable substance, with apparently simple molecular structure that gives rise to many unique properties in condensed phases. Intense scrutiny by spectroscopy, both experimental and theoretical, has not yet resolved all the questions and the vibrational spectroscopy of water ice is no exception. Studies over the past eight decades have revealed Infrared (IR) and Raman spectra of great complexity, largely due to the effects of intermolecular bonding. With the recent discovery of ice XVI [1] there are now 17 experimentally established crystalline phases together with three amorphous phases, each with its own characteristic vibrational spectrum with subtle differences. The focus of this paper will be crystalline ice I_c (cubic) which is the predominant phase of ice particles synthesized under the experimental conditions described below.

Water is a non-linear triatomic molecule with three normal vibrational modes in the gas phase: ν_1 3657 cm^{-1} (symmetric stretch), ν_2 1595 cm^{-1} (bend) and ν_3 3756 cm^{-1} (asymmetric stretch). As water is converted to the liquid phase, these modes are transformed and additional bands appear in the IR spectrum as a result of intermolecular bonding. The distinct ν_1 and ν_3 bands merge into a single, broad OH stretch band with a highly red-shifted wavenumber value. The new bands in the IR spectrum are associated with libration (labelled as ν_L and referring to a frustrated rotation) and lattice modes [2]. Progressing from liquid to solid, the stretching bands within ice are further red-shifted and shoulder features become more pronounced due to contributions from different phonon bands. Phonon modes are collective excitations of periodically arranged molecules and can be described as either acoustic (displaced in the same direction) or optical (alternating direction of displacement). Also, the direction of propagation of the phonon can either be longitudinal (parallel) or transverse (perpendicular) to the direction of the displacement of the phonon. Consequently, the two lattice bands in the far-IR spectrum of ice are labelled as follows: TO (transverse optic) and LA (longitudinal acoustic) [3-5], although there is still some uncertainty on the assignment of these bands [6]. Furthermore, molecules on the surface layers of ice particles that are not tetrahedrally co-ordinated produce dangling bands (dOH/dOD) [7]. Band assignments from the literature for each isotopologue in the gas, liquid and crystalline phases are summarised in **tables 1a, b and c**. A more extensive list can be found in **Tables S1a-c** in the supplementary data.

In addition to the fundamental scientific motivation of understanding its complex spectra, ice is relevant to our atmosphere (ice particles in clouds) and plays a large role in atmospheric processes such as radiative forcing [8]. Ice is also abundant in interstellar media with sources of ice being found from large comets, to ice coatings on small interstellar dust grains [9]. However, the IR spectra of these natural ices are very difficult to interpret without experimental data and thus laboratory molecular ices are synthesized in order to emulate interstellar or atmospheric ices using methods to create ices such as thin films on cold surfaces or as particles.

Table 1a Literature wavenumber values for the vibrational bands of H_2O in the gas, liquid, amorphous solid and crystalline (I_h/I_c) phases. Aerosol particles are predominantly crystalline for diameters > 5 nm.

Phase	Ref.	T (K)	ν_1 , ν_3	ν_2	ν_L	dOH	TO	LA
Aerosol	[10]	80	3228	--	--	--	--	--
		110	3257	--	--	--	--	--
		170	3252	--	--	--	--	--
Aerosol (12 nm)	[11]	100	3255	--	--	3676	--	--
Aerosol (3 nm)		100	--	1658	842	--	--	--
Aerosol (in He)	[3]	5	--	--	--	--	233	166
	[12]	78	3223	1650	*ca*. 850	3690	--	--
Aerosol (in He)	[7]	80	--	--	--	3692	--	--
Aerosol (in N_2)		80	--	--	--	3677	--	--
Aerosol (in N_2)	[3]	200	--	--	--	--	225	157
	[12]	209	3253	1650	860	--	--	--
Amorph. Film	[7]	15	--	--	--	3720 2cs[b]	--	--
		60	--	--	--	3696 3cs[b]	--	--
	[11]	100	--	1671	770-810	--	--	--
	[13]	20	3210	1550	835	--	--	--
		120	3220	1555	828	--	--	--
Cryst. Film	[14]	12	--	--	842	--	--	--
	[15]	78	3240	1585	847	--	--	--
	[16]	78	--	--	--	--	233	230
	[17]	218	3240	1650	820	--	--	--
		258	--	1650	800	--	--	--
	[13]	15	3295	1660	732	--	--	--
		120	3245	1645	785	--	--	--
Cryst. Film (H_2O in D_2O)	[18]	90	3224, 3270	1735	840	--	--	--

	[14]	90	--	--	817/735	--	--	--
Liquid	[19]	292	--	--	--	--	300[a]	80[a]
	[20]	298	--	1638	--	--	--	--
	[21]	300	3405	1651	698	--	--	--
		348	3437	1651	682	--	--	--
Vapour	[22]		3657, 3756	1595	--	--	--	--

[a] Determined using the imaginary component (*k*) of the refractive index from thin film data.

[b] 2cs and 3cs represent 2-co-ordinated and 3-co-ordinated surface molecules respectively.

Table 1b: Literature wavenumber values for the vibrational bands of HOD.

Phase	Ref.	T (K)	ν_1	ν_2	ν_3	ν_L	dOD
Aerosol (18 % HOD in H_2O 4, 6, 7, 8 nm)	[23]	100	2415 (sub-surf)	--	--	--	--
Aerosol (18 % HOD in H_2O 40 nm)			2419	--	--	--	--
Aerosol (18 % HOD in H_2O)	[11]	100	--	1455	--	--	--
Aerosol (50 % H to 50 % D 8 nm)			--	1215	--	--	--
Aerosol in He (HOD in D_2O 12 nm)	[14]	80	--	--	--	824/850	--
Aerosol in He (HOD in H_2O 12 nm)			--	--	--	506/515	--
Amorph. Film (0.5 % in D_2O)	[24]	70	--	--	3297	--	--
Cryst. Film (18 % HOD, 81 % H_2O)	[15]	78	2417	--	--	--	--
Cryst. Film (30 % HOD in D_2O)	[18]	90	2417	1510	--	--	--
Cryst. Film (30 % HOD in H_2O)			--	1490	3270	--	--
Cryst. Film (50 % HOD)	[15]	78	--	1450	--	--	--
Cryst. Film (50 % HOD, 25 % H_2O)			2388	1449	3192	--	--
Cryst. Film (52 % HOD, 49 % H_2O)			2381	1477	3192	819	--
Cryst. Film (9.5 % HOD, 90.25 % H_2O)			2415	--	--	--	--
Cryst. Film (HDO in D_2O)	[25]	100	--	--	3277	822	--
Cryst. Film (HDO in H_2O)			2421	--	--	515	--
Cryst. Film (HOD in D_2O)	[26]	80	2425	--	3272	--	--
Liquid	[27]	283	--	--	3393	--	--
Liquid	[20]	298	--	1469	--	--	--
Liquid (10 % H to 90 % D)	[21]	298	2471	1457	3390	--	--
Liquid (29.8 % D_2O and 25.6 % H_2O)	[20]	298	--	1446	--	--	--
Liquid (50 % H to 50 % D)	[21]	298	2493	1457	3391	--	--
Liquid (90 % H to 10 % D)			2499	1457	3377	--	--

Liquid ('pure' HOD)	[20]	298	2485	1439	3370	--	--
Nanocryst. (18 % HOD in H_2O)	[28]	136	--	--	--	--	2713
Vapour	[29]		2724	1403	3707	--	--

Table 1c: Literature wavenumber values for the vibrational bands of D_2O.

Phase	Ref.	T (K)	ν_1 , ν_3	ν_2	ν_L	dOD	TO	LA
Aerosol	[10]	80	2428	--	--	--	--	--
	[30]	100-145	2438[a]	--	--	--	--	--
Aerosol (12 nm isolated in H_2O)	[14]	90	--	--	453/504/525	--	--	--
Aerosol (12 nm)			--	--	628/663	--	--	--
Aerosol (16 nm)	[23]	100	2430	--	--	--	--	--
Aerosol (8 nm)	[11]	100	--	1211	--	--	--	--
Amorph. Film	[7]	15	--	--	--	2748 2cs[b]	--	--
			--	--	--	2727 3cs[b]	--	--
Amorph. Film	[23]	80	2459	--	--	--	--	--
Amorph. Film (HOD in D_2O)	[31]	80	--	--	--	--	--	--
Amorph. Film (in He)	[7]	15	--	--	--	2749 2cs[b]	--	--
			--	--	--	2729 3cs[b]	--	--
Amorph. Film (in N_2)		15	--	--	--	2725 2cs[b]	--	--
			--	--	--	2707 3cs[b]	--	--
Cryst. Film	[16]	78	--	--	--	--	227	--
	[14]	90	--	--	633/661	--	--	--
	[17]	103	2450	1210	630	--	--	--
	[25]	110	2425	1210	640-675	--	--	--
	[32]	110	2524	1214	--	2728	--	--
Cryst. Film (2 % D_2O in H_2O)	[18]	90	2366, 2444	1225	640	--	--	--
Cryst. Film (D_2O on H_2O)	[33]	145	2425	--	--	--	--	--
Low Density Amorph. Film	[24]	70	2435[c]	--	--	--	--	--
Liquid	[34]	278	2475	1217	--	--	--	--
	[17]	283	--	--	530	--	--	--
	[35]	298	2500	1210	--	--	--	--

Liquid ('pure' D_2O)	[20]	298	2484	1214	--	--	--	--
Vapour	[36]		2672, 2788	1178	--	--	--	--

[a] The sub-surface position determined by subtracting a spectrum at 145 K from 100 K.

[b] 2cs and 3cs represents 2 co-ordinated and 3 co-ordinated surface molecules respectively.

[c] Determined using the imaginary component of the dielectric constant ε (= $2nk$) from thin film data.

Thin films and particles

Thin film studies present certain advantages such as: the availability of many instruments that are capable of performing vapour depositions; generation of samples that are representative of the bulk material; stable conditions in which to grow and maintain the ices and hence more time to gather data; the ability to control thickness and whether multiple samples are deposited separately or simultaneously. It should be noted that slow deposition of water vapour onto a cold substrate below 110 K leads to a more disordered phase known as low density amorphous ice. It has band positions and shapes that differ from those in I_c, however a transition to the crystalline phase is possible by annealing to temperatures above 135 K where the glass transition occurs. Spectra of molecular ices synthesized using these techniques suffer from optical effects that depend on the thickness of the film because of the wavelength dependence of the refractive index. Sample-substrate interactions are also possible which may further distort and shift spectral lines.

An alternative technique, collisional cooling [12, 37-39], is employed in the present study to produce nanoscale ice particles ranging from 20 – 500 nm in diameter. This is advantageous as it avoids generating particles that are either too small (e.g. supersonic jet expansion [40]) where vibrational features from disordered surface molecules dominate the IR spectra; or too large (e.g. electrospray [41-43] and acoustic levitation [44, 45]) where scattering contributions from the real (*n*) component of the refractive index becomes significant. Furthermore, particulate ices are more representative (in terms of size and shape) of particles found naturally in clouds and interstellar media when compared to vapour deposited flat samples and thus their spectra are more directly comparable. Furthermore, parameters extracted from such spectra yield more accurate prediction models. Naturally, size effects must be accounted for, and for spectra of large particles (with diameters $\geq \lambda / 10$, or *ca*. 0.5 μm in diameter for full mid-IR spectra) contributions from short-wave scattering become increasingly substantial and require meticulous data processing in order to remove this contribution. At the small end of the scale, particles of less than ≈ 20 nm show a significant spectral contribution from strained surface molecules and a disordered core occurs for diameters less than 4 nm [46]. In the size regime of 20 - 200 nm [12], ice nanoparticle spectra are relatively unaffected by such spectral and optical distortions, but still present spectra from which bulk ice spectra can be derived [47].

Temperature effects

It is known that the wavenumber values of the IR bands of ice shift with size and temperature [26]. As temperature decreases: thermal population of excited vibrational levels is reduced; the ice volume is decreased and intermolecular H-bonds are strengthened. This results in blue-shifted wavenumber values for the ν_L libration and ν_2 bending bands due to their vibrational motion becoming more restricted, and a red shift in the OH stretch band as the intramolecular O-H bond weakens. The thermally induced shift in the OH stretch band is particularly marked, ≈ 0.2 cm^{-1} K^{-1} [12] such that it could be used as a proxy for temperature. A question that arises however, is just how much of that temperature gradient is due to the intrinsic change in the force constants due to the weakening of the H-bonds with increasing temperature, and how much is due to the associated changes in mode coupling between molecules. This provides part of the motivation for our reassessment of the temperature dependant wavenumber values for all vibrational bands, and consideration of the effects of Fermi resonance and phonon coupling using isotopic dilution.

Theoretical studies

Computational studies can provide valuable insights to help interpret such spectroscopic behaviour as a valuable complement to experiments. Molecular dynamics (MD) is often the method of choice for ice because it is capable of computing large arrays of molecules which is important for modelling bulk properties of ice. Some applications of MD include, but are not limited to investigating: proton tunnelling in I_h [48]; the length and elongation of phonon modes [49]; approximating wavenumber shifts due to temperature [50] and isotopic dilution [51]; intensity differences due to phase changes [52] and the anomalous behaviour of water ice under mechanical compression and thermal excitation [53, 54]. Recently, Skinner *et al*. developed a mixed quantum/classical approach for modelling the OH (OD) stretch vibrational spectroscopy of water in its condensed phases [55-60]. Specifically for ice, the model has been vigorously tested and compared with experimental IR, Raman, 2D-IR, pump-probe, and inelastic incoherent neutron scattering data of pure of mixed hexagonal ices [58-63]. Some results for cubic ice from this model are compared to our nanoparticle experimental data in the work presented below.

Isotopic dilution

In order to assist the interpretation of the complex spectra of pure ices, one can manipulate the molecular ice by distributing small amounts of H_2O in an inert gas matrix [64] or by depositing isolated H_2O molecules on D_2O [32]. The former method simplifies the spectrum by removing the intermolecular bonds entirely, although ro-vibrational transitions can still be observed in some spectra [65]; the latter approach which consists of H_2O deposition onto pre-deposited D_2O [32] can be an effective method for isolating H_2O molecules while still maintaining the H-bonding interactions. If a sample is deposited at temperatures below 145 K, proton exchange is not observed on the surface layers between H_2O and D_2O [33]. In earlier works by Devlin and co-workers [18, 66], spectra for intact isolated D_2O [18] and H_2O [66] were reported showing clearly resolved peaks for the ν_1 and ν_3 OD/OH stretches. Separate deposition of the samples proves advantageous if one wants to avoid making HOD (**Equation 1**), which is formed as a result of the equilibrium between H_2O and D_2O [20].

$$H_2O_{(l)} + D_2O_{(l)} \rightleftharpoons 2HOD_{(l)} \qquad K_e \approx 3.76 \text{ to } 3.94 \text{ at } 25\ ^\circ\text{C} \qquad (1)$$

Formation of HOD by pre-mixing solutions or co-deposition also has its own benefits, in particular for measuring the dynamics of intermolecular bonding in solutions [67, 68]. However, the main advantage of producing HOD diluted in either D_2O (or H_2O) is its effectiveness in isolating and therefore vibrationally decoupling the OH (or OD) oscillator of HOD [18]. The resulting localised excitation greatly simplifies that part of the IR spectrum and can therefore help with interpretation of the underlying physics, a strategy that has been applied to conventional IR spectroscopy [18, 21, 69] and with 2D and 3D techniques [26, 31]. Advantageously, the ν_3 band of HOD should be located approximately in between the ν_1 and ν_3 bands of decoupled H_2O and similarly for the ν_1 of HOD and D_2O.

While pure D_2O and mixed molecular ices of dilute HOD have been subject to spectroscopic studies, most of these have concerned thin films with a limited number focussing on particulate ices. Devlin

[10] reported the first spectra of both crystalline and amorphous micro-particle ices of H_2O, D_2O and mixtures in the hydride stretch region with the amorphous ice bands blue-shifted from the crystalline bands by some 10 - 30 cm^{-1}, see **Tables 1a-c**. The dangling band of amorphous ice is also blue-shifted due to the highly disordered surface layers and transitions to a doublet band [70] which is assigned to the 2 (2748 cm^{-1}) and 3 co-ordinated (2727 cm^{-1}) surface D_2O molecules [7]. However, in the presence of adsorbate molecules such as H_2, Ar or N_2, the dangling band can be red-shifted up to 20 cm^{-1}. For nanoparticles ≤ 16 nm in diameter, surface and subsurface molecules contribute strongly to the overall intensities and band shapes, along with the core. Even in 16 nm diameter D_2O particles, it is estimated that more than 25 % of the OD stretching band comes from surface and subsurface molecules [23]. The surface contribution is also clearly evident in the sharp band feature near 1650 cm^{-1} associated with the bending mode of surface H_2O molecules which is superimposed over the broad $\nu_2/2\,\nu_L$ absorption [11]. Serendipitously, the ν_L band is influenced only in small particles [14].

The present study explores the IR spectroscopy of nanoscale particulate ice in the stretch, bend and libration regions. We systematically examine the effects of both temperature, and of varying isotopic concentration, where some intriguing differences emerge between the OH and OD stretching regions. Complementary molecular dynamics calculations explore the temperature and isotope effects in this region of the spectrum.

Experimental

The instrumental setup is described in detail elsewhere [3, 12]. Briefly, spectra were recorded at the Australian Synchrotron THz/Far-IR beamline using a Bruker IFS125/HR spectrometer coupled to an enclosive flow cooling (EFC) cell [72]. The internal globar was used as the light source and the spectrometer was fitted with a KBr beamsplitter; KBr windows were also used on the EFC cell. Spectra covering the full bandwidth (550 - 5000 cm^{-1}) were recorded using a MCTm (mercury cadmium telluride mid band) detector at a resolution of 1 cm^{-1}. A Blackman-Harris 3-Term apodization function with a zero fill factor of 2 was used in the Fourier transformation of the data.

Distilled H_2O and D_2O (99.9 % Merck) were used without further purification to make the H_2O-D_2O mixtures. Aliquots of either H_2O or D_2O were portioned into a steel cylinder (*ca*. 100 mL) using either a 5 mL or 10 mL disposable syringe. Helium gas was flowed through the bubbler to minimise contamination from atmospheric CO_2, N_2 and H_2O whilst the liquids were being added. The container was then gently swirled once the top had been placed on. For each mixture, helium was slowly bubbled through the system toward the pump for *ca*. one minute (bypassing the EFC) to establish an equilibrium between the adsorption and desorption of H_2O/HOD/D_2O molecules onto the nylon tubing and bubbler walls.

For an experiment at 180 K, the EFC cell was filled with 20 kPa He buffer gas and left to thermally equilibrate for *ca*. two minutes. During this time, the steel bubbler was pressurised with 275 kPa He carrier gas. The helium gas flow was then isolated and the He-H_2O/HOD/D_2O gas mixture was left to equilibrate for *ca*. one to two minutes. A control background spectrum was recorded once the temperature of the EFC cell had stabilised and a set of 400 scans (200 files with 2 scans per file) was initiated using Bruker's OPUS 6.0 software to record the spectra resulting from a single pulse (1000 ms) of the equilibrated He-H_2O/HOD/D_2O gas mixture that was introduced into the EFC cell. Spectra of nanoparticle formation was recorded over a time period of approximately six minutes as particles were formed and diffused through the optical beam, with the final averaged spectrum consisting of spectra taken after a short delay (< two seconds) to allow for the complete formation of nanoparticles. Upon completion of the 400 scans, the EFC cell was evacuated to remove the sample and a second control background spectrum was recorded to monitor any ice that had adsorbed onto the surface of the bottom mirrors. Spectral contributions emanating from ice adsorbed onto the mirrors were removed via spectral subtraction of the adsorbed ice from the final averaged spectrum.

The central temperature of the cell was monitored using an iron-rhodium thermistor, whereas k-type thermocouples were used for the colander (top, middle and bottom positions) as well as the top and bottom mirrors. The heater temperatures for the mirrors were maintained approximately 10 K above the colander temperatures in order to minimise ice adsorption and the central cell temperature was recorded before and after each experiment. This process was repeated for each measured temperature in the temperature series down to 7 K. Three different coolants were used in the outer jacket of the EFC cell for the different temperature ranges: liquid helium for temperatures below 78 K, liquid nitrogen for temperatures between 78 – 150 K and cold nitrogen gas for 130 - 190 K.

For the dilution series, the experimental conditions used are as given above, except that the detector was changed to a MCTn (narrow band) which has a more restricted low wavenumber cut off of 700 cm^{-1}.

Computational

The OH (OD) stretch IR spectra were modelled using a mixed quantum/classical approach developed by Skinner and co-workers [73]. In this method, the OH (OD) stretches are treated quantum mechanically, while the translational and rotational degrees of freedom are described by classical molecular dynamics (MD) simulations using rigid water models and the intra-molecular bends are ignored. The detail of this method, including the *ab initio*-based spectroscopic maps used in this work, is discussed in ref. [58]. One noteworthy point about this method is that the intramolecular and intermolecular OH (OD) vibrational couplings are explicitly considered when there are multiple OH (OD) chromophores in the systems (e.g. neat H_2O ice).

The MD simulations were performed for bulk cubic ice instead of cubic ice nanoparticles in that their experimental IR spectra are very similar (except for the dangling OH or OD peak) provided that the diameter of the ice nanoparticle is greater than 8 nm [12]. The initial proton-disordered configuration for cubic ice is a 216-molecule configuration from ref. [74]. It is known that at 88 K the density of cubic ice is almost identical to that of hexagonal ice [75], but only the temperature dependence of the latter is well documented [76]. Therefore, the cubic simulation box was scaled to match the experimental density of hexagonal ice at a given temperature (e.g. 10, 80 and 200 K). The system then was simulated in a NVT ensemble using the explicit three-body (E3B) water model recently developed by Skinner and co-workers [77]. All simulations were performed with a modified GROMACS package 4.5.5 [78]. Other simulation details are identical to those in Ref. [58] except that in this work the MD trajectories were saved every 5 fs in the production runs for the spectral calculations.

For the spectral calculations of the $H_2O/HOD/D_2O$ mixtures with % OD < 50 %, after running the MD simulations for H_2O, we assigned the H atoms to be D atoms at random based on % OD (this is equivalent to the assumption of the equilibrium constant in **Equation 1** to be 4.00, which is close to the experimental value for liquid water [20]). Likewise, for the $H_2O/HOD/D_2O$ mixtures with % OH < 50 %, the D atoms from the D_2O simulations were randomly assigned to be H atoms. For each mixture, an average over 400 different random realizations was performed to guarantee the spectral convergence.

Results and discussion

Peak maxima vs centre of gravity (COG)

Unless stated otherwise, the wavenumber values given herein are obtained using a method for estimating the COG position (**Equation 2**), rather than the conventional peak max method due to the broad, asymmetric nature of the vibrational bands.

$$\text{Peak position}_{\text{COG}} = \frac{\int \bar{\omega} A(\bar{\omega})\, d\bar{\omega}}{\int A(\bar{\omega}) d\bar{\omega}} \qquad (2)$$

where $\bar{\omega}$ is in cm^{-1}

The (default 90 %) COG wavenumber value is calculated using the peak picking procedure in Bruker's OPUS 6.0 software with upper and lower integration limits for $\bar{\omega}$ such that $A(\bar{\omega}) = 0.1A_{max}$. Spectra were re-transformed at 4 cm^{-1} resolution in order to minimise noise which affected the COG and peak max wavenumber values of the ν_L libration and OH/OD stretching bands. Plots shown below do not include data points for temperature between 58 - 78 K because it was difficult to maintain stable temperatures within this range. Some data points do not have error bars as they are too small to be included.

Particle size

The average particle diameter observed throughout the experiments ranges from 10 nm at 7 K to 40 nm at 150 K. Beyond that, they are larger still. Average particle sizes, **Figure 1**, are determined by comparing the integrated intensity of the dangling OH or OD bands (dOH or dOD) with their respective hydrogen-bonded stretch bands, and accounting for the N_2 adsorption observed at temperatures less than 60 K [46]. Short-wave scattering is also observed in some of our experiments, and although conventionally used for thin film ices [79] it can also be used to estimate particle sizes as diameters approach λ / 4π at warmer temperatures, where λ is the wavelength in nm. Although not shown on the scale in **Figure 1**, particles can reach diameters of *ca*. 300 nm diameter at 200 K. The scattering is measured at *ca*. 4000 cm^{-1} and then compared to calculations based on a discrete dipole approximation (DDA) [80]. It is also assumed that the size distribution of the particles follows a log normal distribution.

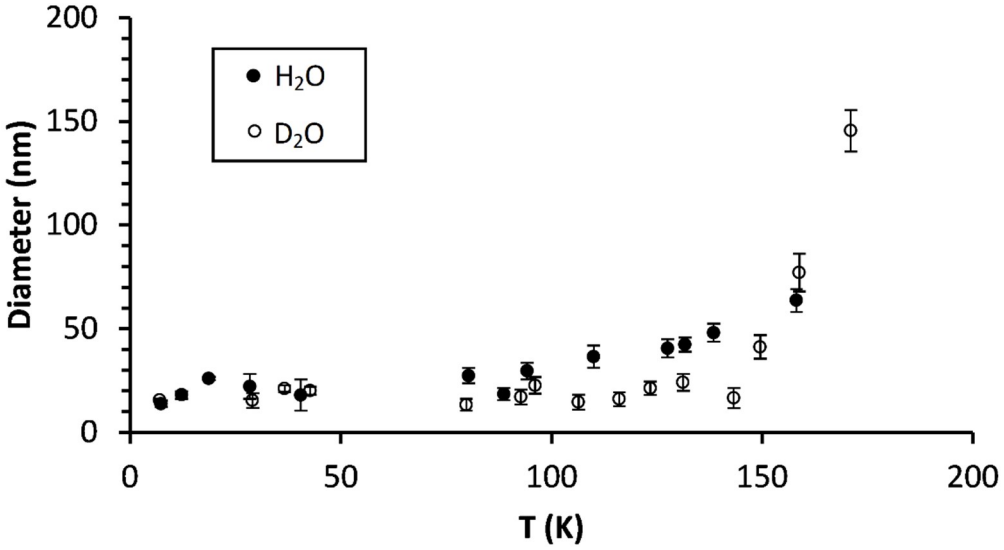

Figure 1: Average particle diameters for mostly pure H_2O (filled) and D_2O (open) nanoparticles. The larger error bars for particles below 60 K result from taking account of N_2 adsorption.

Spectra and analysis of the vibrational bands

A mid-IR survey spectrum of ice nanoparticles at 78 K between 550 - 4000 cm^{-1} is provided in **Figure 2**. The % OH and % OD values cited throughout refer to the molar percentage of all the hydrogen atoms that are protium and deuterium, respectively. They can be approximately evaluated using **Equations 3a-c**.

$$\%\mathrm{OD} = \frac{\sqrt{2} f I_{OD}}{1+(\sqrt{2}-1) f I_{OD}} * 100 \qquad \textbf{(3a)}$$

$f I_{OD}$ is the fraction of total hydride stretch intensity in the OD region, given as

$$f I_{OD} = \frac{I_{OD}}{(I_{OH}+I_{OD})} \qquad \textbf{(3b)}$$

$$= \frac{\%OD}{\%OD+\sqrt{2}(100-\%OD)} \qquad \textbf{(3c)}$$

where I_{OD} and I_{OH} are the integrated intensities in the OD and OH stretch regions respectively.

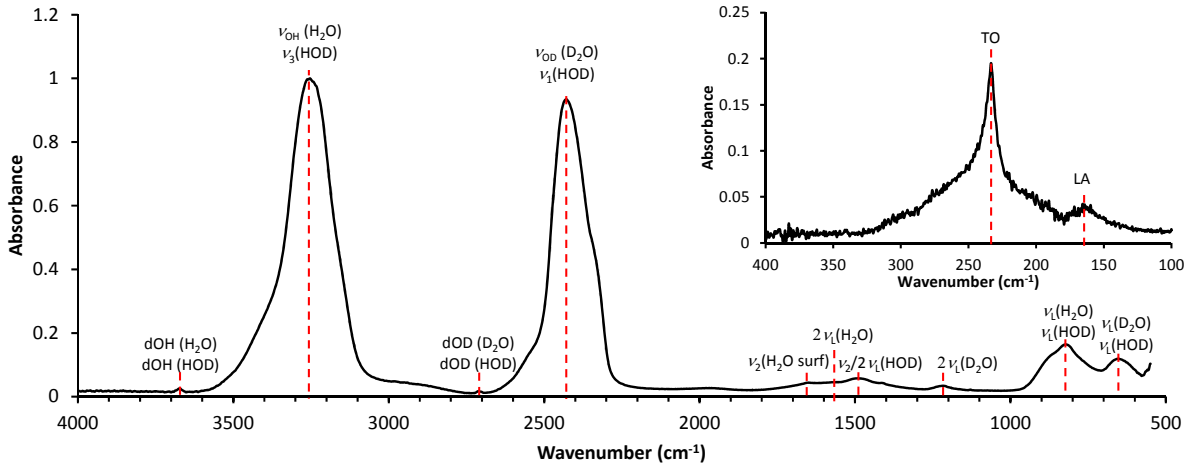

Figure 2: A normalised mid-IR survey spectrum between 500 - 4000 cm^{-1} of ice nanoparticles with *ca*. 51 % OD at 78 K. The inset shows the far-IR spectrum of pure H_2O ice nanoparticles at 80 K.

It is clear that many of the vibrational bands are still very broad even with isotopic dilution and **Figure 3** shows the evolution of the ν_L and $\nu_2/2\,\nu_L$ bands of each species as % OD is increased from ≈ 3 % starting at the top trace. Each isotopologue contributes its own set of intramolecular vibrations, but these along with the intermolecular modes may be affected by coupling to the surrounding molecules (see for example the ν_2 mode of HOD which differs slightly in D_2O and H_2O matrix). Estimations for the positions of the overtone bands of ν_2 and ν_L are given in **Table S2** of the supplementary data. Further broadening within the mid-IR region results from the addition of thermally excited hot bands. Given that the mid-IR spectra of I_h and I_c are identical, we assume that the nanoparticles in this study consist of the latter phase as it is kinetically favoured [81-83] and has a faster nucleation rate [84] at the temperatures employed in this study. The shapes of particles are also assumed to be spherical [46].

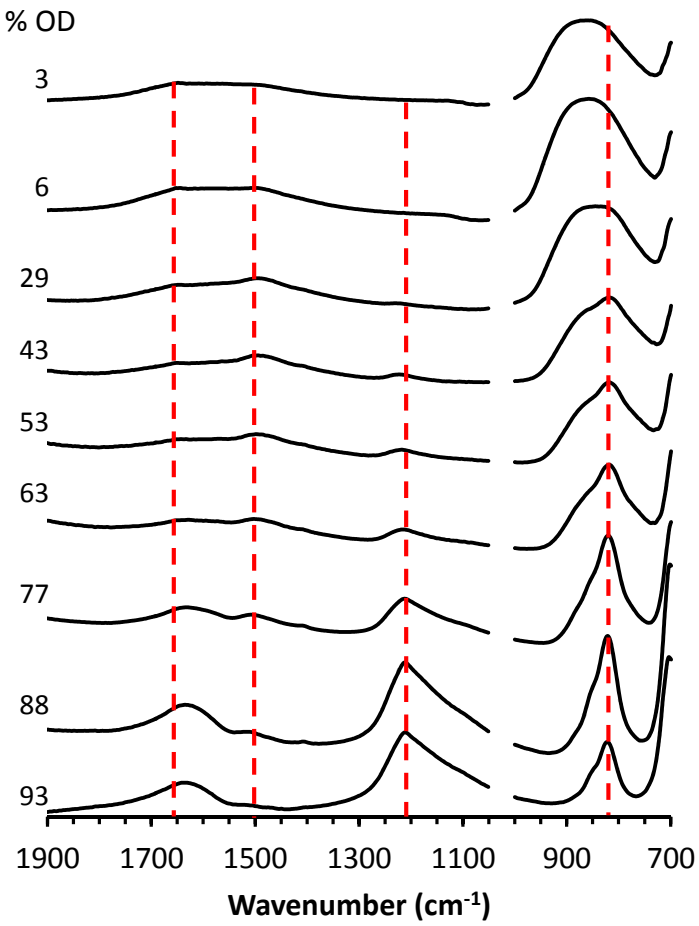

Figure 3: Changes in the mid-IR spectrum of ice particles between 700 - 2000 cm^{-1} as % OD increases. A small peak from residual isopropanol impurity between 1050 - 1000 cm^{-1} has been removed.

Libration (ν_L) vs temperature and isotopic concentration

The ν_L band of H_2O particles has a broad and flat top structure with a peak maximum near 867 cm^{-1} at 7.4 K. As the temperature is increased from 7.4 to 195 K, the ν_L band is red-shifted by only 15 cm^{-1}, corresponding to a modest, negative gradient of *ca*. - 0.08 cm^{-1} K^{-1}. These results are comparable to those previously reported by Severson *et al*. [14], where the ν_L band of crystalline H_2O clusters at 90 K (with diameters ≈ 12 nm) is located at approximately 868 cm^{-1}. In the context of aerosol particle spectra, the ν_L band is shifted much more with decreasing size (and greater surface contribution) [12, 14] than directly by temperature effects and hence the decrease in particle size below 50 K is probably the cause of the flatter curve at the coolest temperatures. There is a significant difference of *ca*. 30 cm^{-1} between crystalline aerosol and thin film data [13, 14], though the temperature gradient is similar. Even with particles sizes large enough to undergo scattering related red-shift in wavenumber value (*ca*. 0.6 μm in diameter) the ν_L band positions observed by Clapp *et al*. [85] are still higher than in the thin film, see **Figure 4**. The temperature trend and gradient for the libration band of D_2O mirrors that in H_2O, although the wavenumber values of $\nu_L(D_2O)$ below 50 K are anomalous (**Figure S1** in the supplementary data) because of the increased noise levels near the detector low wavenumber cut-off.

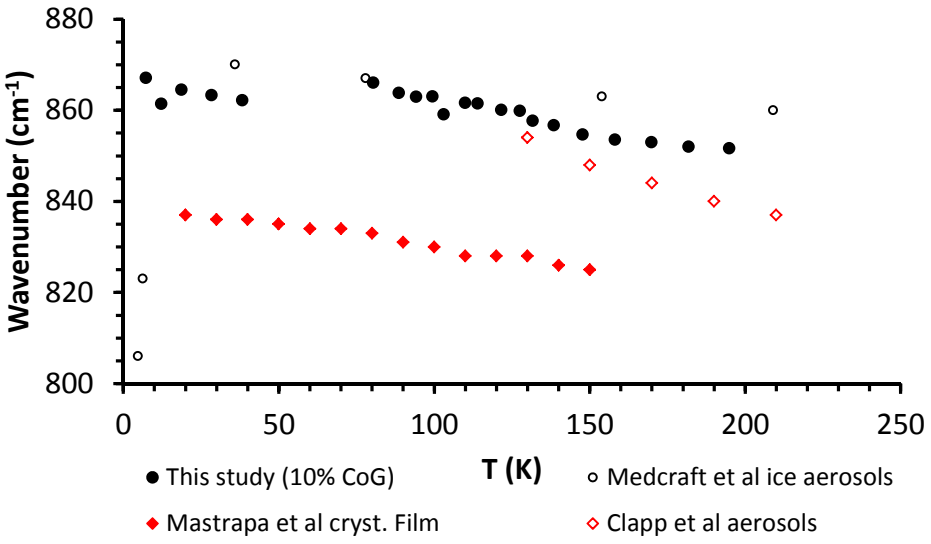

Figure 4: Peak position of the $\nu_L(H_2O)$ band showing the red-shift with increasing temperature. The present data is obtained by COG integration of only the top 10 % of the peak, corresponding to the integration limit $A(\bar{\omega}) = 0.9A_{max}$.

At 78 K, the relatively featureless ν_L bands for pure H_2O and D_2O are located near 866 and 655 cm^{-1} respectively. Both bands are fairly symmetrical with differing full-width half-max (FWHM): 160 ± 5 cm^{-1} for H_2O and 91 ± 5 cm^{-1} for D_2O. As % OD increases, the FWHM of the $\nu_L(H_2O)$ band is decreased linearly to *ca*. 50 cm^{-1}. Also, the band becomes more structured and is red-shifted to 827 cm^{-1} (see bottom trace in **Figure 3**). In this situation, the ν_L band is most likely emanating from HOD rather than H_2O as pointed out in Buch's study (827 cm^{-1} for isolated HOD in D_2O) [14], and is reassigned to $\nu_L(HOD)$. The $\nu_L(D_2O)$ band shift is not observed as it is below the 700 cm^{-1} ~~MCTm~~ cut-off of the MCTm detector, however it is expected that a similar trend occurs given that the wavenumber values of D_2O/HOD isolated in H_2O have previously been reported to be near 525 and 515 cm^{-1} respectively [14].

Bending mode (ν_2) vs temperature and isotopic concentration

H_2O

In the ν_2 bend region also, the profile of H_2O bands changes markedly with both temperature and size. For particles with "large" (i.e. greater than ≈ 40 nm) diameter at 78 K, the peak maximum is located around the centre of the very broad (FWHM ≈ 320 cm^{-1}) band at *ca*. 1580 cm^{-1} (**Figure S2** in the supplementary data). Around 140 K, the peak maximum shifts and a shoulder feature appears on the high wavenumber side at 1649 cm^{-1}. The trend is consistent with the crystalline thin film data of Mastrapa *et al*. [13], with the band maximum position changing from 1564 cm^{-1} at 20 K to 1624 cm^{-1} at 150 K. This contradicts the expectation that the ν_2 band will be red-shifted as temperature is increased due to weakening of intermolecular hydrogen-bonds and reduction in the intramolecular H-O-H angle [52]. It also runs counter to the observation that increasing temperature shifts the peak position of every other band of crystalline ice towards the corresponding amorphous solid or liquid band.

The apparently anomalous trend only makes sense in the context of the overlapped and Fermi mixed $\nu_2/2\,\nu_L$ character of the band, as outlined by Devlin and co-workers [11, 86]. The $2\,\nu_L$ overtone in this region displays the same broad character as the ν_L fundamental band and has sufficient intensity that it can obscure the ν_2 contribution. In marked contrast to the OH stretch modes, IR intensity of the bending mode decreases with hydrogen-bonding and is particularly weak for low temperature crystalline ice. In their molecular dynamics study, Imoto *et al*. [52] attributed this to a strong anti-correlation between the permanent dipole moment and the induced dipole moment of its hydrogen-bond acceptor molecule, an effect that is diminished with hydrogen-bonding disorder. The ν_2 band intensity is much greater in the amorphous layer of aerosol particles than the crystalline core, giving rise to the distinctive peak around 1650 cm^{-1} that is clearly evident for particles of diameter up to 20 nm at 100 K [11]. Thus, the apparent blue-shift as the temperature increases is more a consequence of increasing disorder allowing an enhanced ν_2 contribution at the higher wavenumber end of the $2\,\nu_L$ envelope.

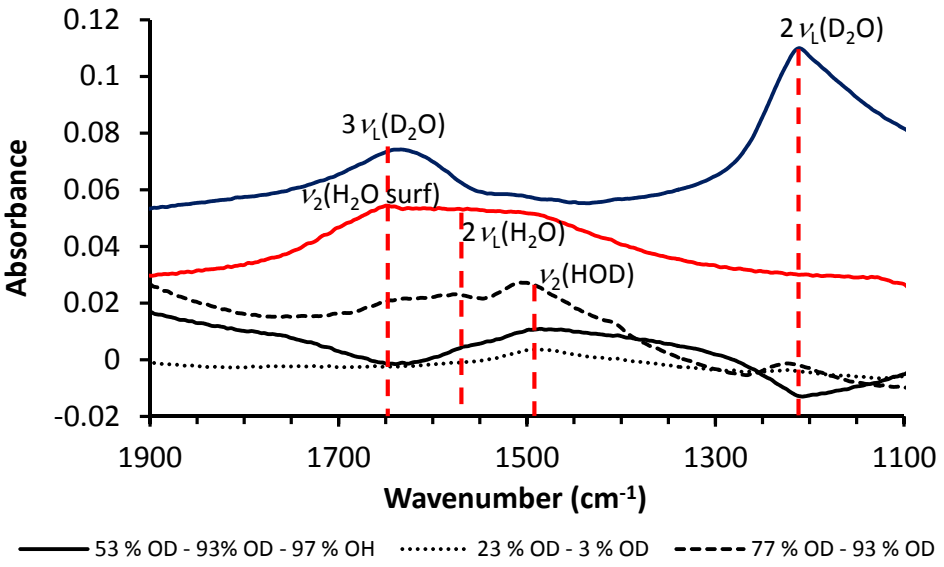

Figure 5: The $\nu_2/2\,\nu_L$ region of H_2O, HOD and D_2O nanoparticles at 78 K. The blue and red traces represent 93 and 97 % OD and OH respectively and are vertically offset for ease of comparison. The three black traces show the notional HOD ν_2 band obtained by subtracting different combinations of spectra.

With isotopic dilution, there is little evidence of a shift in the amorphous 1649 cm^{-1} shoulder as shown in **Figure 3**. It is difficult to observe what occurs with the broad underlying $2\,\nu_L$ band because of overlap with both HOD and with the $3\,\nu_L$ band of D_2O at ≈ 1634 cm^{-1}.

D_2O

The corresponding $\nu_2/2\,\nu_L(D_2O)$ band evident in the blue trace of **Figure 5** has a distinctive asymmetric triangular shape with a long tail toward lower wavenumber values and a FWHM linewidth of *ca*. 145 cm^{-1} which is much reduced compared to H_2O. The peak maximum of 1211 cm^{-1} is barely shifted for temperatures ranging from 7 - 190 K and the band profile is not very sensitive to

particle size. However, isotopic dilution does narrow the band and blue-shift it (e.g. at 80 K and % OD ≈ 43 %, the band peaks at 1223 cm^{-1} and has a FWHM of 50 cm^{-1}. The analysis of Hernandez *et al*. [86] assigns the bulk crystal ν_2 mode to around 1265 cm^{-1}, and hence the observed band to $2\nu_L$.

HOD

HOD is the most difficult isotopologue to characterise in our experiments because it is always present with at least one of the other isotopologues, and at a maximum concentration of ≈ 50 %. At intermediate D/H isotopic ratios, HOD has the highest concentration and a separate feature becomes visible at ≈ 1500 cm^{-1}, on the "red edge" of the $2\nu_L(H_2O)$ band (**Figures 2** and **3**). This band of HOD has an approximately Gaussian shape with a width of *ca*. 70 cm^{-1} depending on temperature and isotopic concentration. By subtraction of spectra with different isotopic ratios, we can derive notional spectra of this HOD band (black traces in **Figure 5**). The reduced linewidth compared to H_2O or D_2O bands tends to support the assertion by Devlin *et al*. [18] that this band is predominantly ν_2 in character. It undergoes only a modest red-shift with temperature (e.g. 1497 cm^{-1} at 78 K to 1494 cm^{-1} at 140 K). More interestingly, the position shifts depending on the isotopic concentration at 78 K to 1487 cm^{-1} in mostly H_2O to 1508 cm^{-1} in mostly D_2O. Observing similar shifts in thin film spectra, Hernandez *et al*. [86] attributes this to Fermi resonance coupling with the libration overtones of the surrounding host species. The cancellation of transition dipole contributions inferred for the ν_2 vibrations of H_2O [52], and by implication D_2O, is expected to occur to a lesser extent in HOD.

OH/OD stretching modes vs temperature

The hydrogen bonded hydride stretch bands of near pure crystalline H_2O and D_2O are shown in **Figure 6**. The sub-structure that is evident includes at least three clearly discernible peaks labelled 2 - 4 for consistency with Shi *et al*. [58] where peak 1 is seen in the Raman but not IR spectra. These features have been interpreted in many, but sometimes contradictory ways, based on different models [58]. In **Figure 6**, the labelling is from firstly, Buch & Devlin's work based on excitations in periodic systems comprised of four oscillating dipoles tetrahedrally arranged around each O-atom [87] and secondly, in square brackets, the recent assignments of Shi *et al*. [58] where S and W refer to strong and weak intermolecular couplings, while H and L simply denote high and low wavenumber. Intramolecular couplings (W(I)) are also present in D_2O, however only W is used in this work for simplicity.

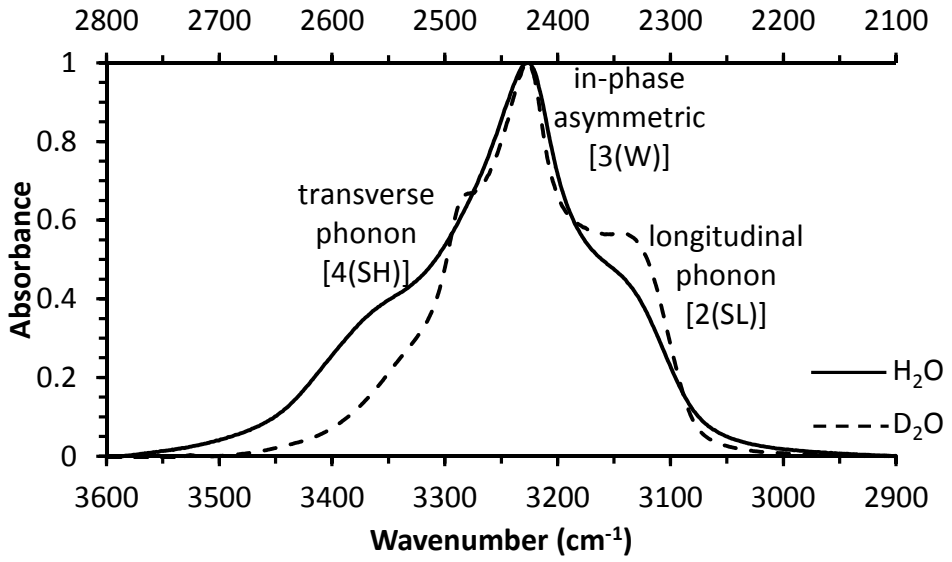

Figure 6: The OH and OD H-bonded bands of almost pure crystalline H_2O and D_2O particulate ices at 78 K. The three observed peaks are labelled using both the phonon mode description of [12, 87] and in square brackets the assignment by Shi *et al*. [58].

Figure 7 compares a series of experimental and MD simulated spectra vs temperature for the OH stretch. Throughout the temperature series, peak 3 (W) in the hydride stretch remains the most prominent feature and the intensity ratios between the three peaks remains fairly consistent. Individual peak components are broadened at higher temperatures but the overall width is little changed. More significantly, the band system is blue-shifted with increasing temperature in contrast to the ν_L, $2\nu_L$ and ν_2 bands. Thermal excitation of low energy intermolecular modes contributes to the weakened longer intermolecular H-bonds and correspondingly strengthened intramolecular O-H/D bonds. This matches the observation of a larger unit cell (and lower densities) at warmer temperatures as explained by Wagner [88], and the lattice mode band positions in the far-IR region do show the corresponding red-shift with temperature [3]. In a recent MD study based on hydrogen (O--H-O) bond co-operative relaxation, Sun *et al*. [49, 53] predicted a blue-shift in the OH stretch phonon of + 50 cm^{-1}, and a red-shift of smaller magnitude (- 15 cm^{-1}) for the lattice mode associated with intermolecular H-bonding over the range of 98 - 258 K. The simulations of **Figure 7** correctly predict the blue-shift with temperature, although the magnitude is somewhat greater than observed.

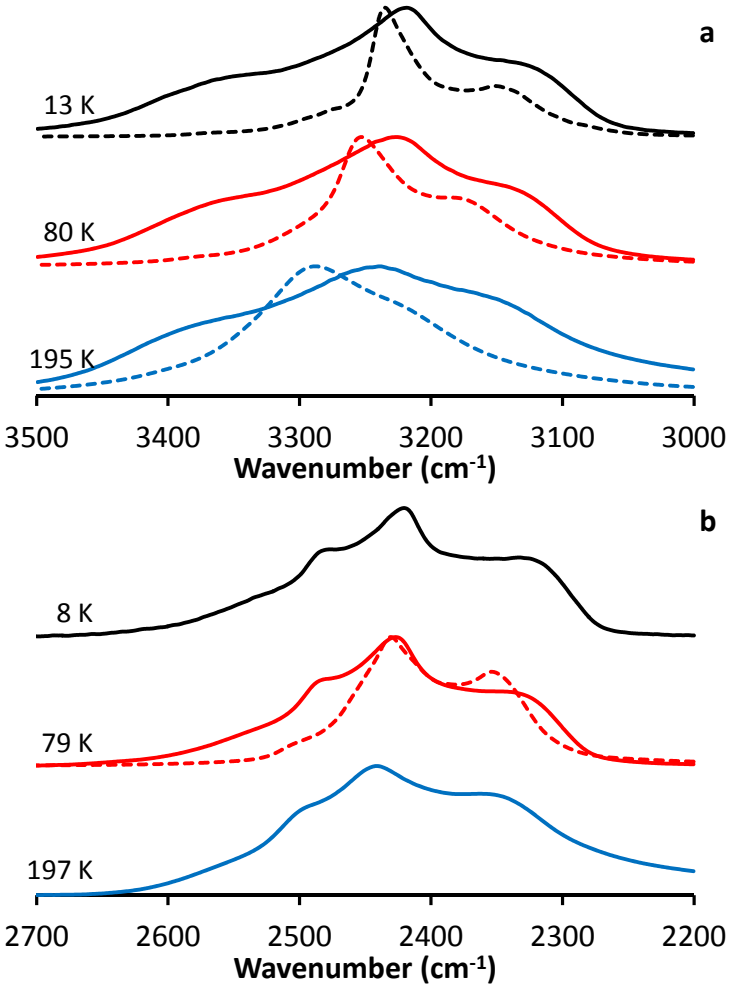

Figure 7: Comparison of the experimental (solid) and calculated (dotted) band shapes and wavenumber shifts for the OH H-bonded stretch for near pure crystalline H_2O in **panel a**. The simulations were performed at 10, 80 and 200 K. **Panel b** shows the same H-bonded stretch, but for near pure crystalline D_2O along with a simulated spectrum at 80 K (dashed line).

Gradients

Figure 8 plots the temperature dependence of H-bonded stretching peaks determined in three different ways to facilitate analysis of the trends. The peak maximum values of the band system, corresponding to the position of peak 3, follow a linear trend. The positions of peaks 2 and 4 for both near pure H_2O and D_2O were also determined, by using the second derivative function in OPUS and reducing the resolution of the spectra to 8 cm^{-1}. The positions of peaks 2, 3 and 4 are all blue-shifted at very similar rates, with gradients corresponding to 0.14, 0.12 and 0.12 cm^{-1} K^{-1} respectively. The gradient of the shift is slightly less than previously reported [12, 58] due to lower wavenumber values from spectra with T > 150 K. This may be accounted for by some larger particle sizes for the present set of experiments as discussed below.

In near pure D_2O, a similar trend is observed where peaks 2, 3 and 4 are all linearly blue-shifted with increasing temperatures. The differences in gradients for all three peaks are slightly larger for the H-bonded OD stretch, compared to OH, and their calculated gradients are 0.16, 0.11 and 0.10 cm^{-1} K^{-1} respectively. The larger gradient for peak 2 is due to the increased widths at higher

temperatures, as seen in the blue trace of **panel b** in **Figure 7**, which has a strong influence on the second derivative position. Taking this into account, it is clear that the gradients for peaks 2, 3 and 4 are almost the same, both in H_2O and in D_2O.

The COG measurements, corresponding to the mean position of the entire band system, are blue-shifted at slightly smaller gradients of 0.09 cm^{-1} K^{-1} (for OH) and 0.05 cm^{-1} K^{-1} (for OD) and reflects the influence of the two SL and SH phonon bands. In particular, the SL band has a long tail that extends to lower wavenumber values on the red edge of the OH and OD stretching bands (**Figure 7**). Larger particles at warmer temperatures (e.g. > 130 K) also show increased intensities for the two phonon bands, which further red-shifts the COG band position, leading to a smaller gradient. We estimate the upper limit of particle sizes can be estimated by comparing observed short-wave scattering to predictions from simulations formed within our group using refractive index data [85]. At 130 K, the scattering profile in some spectra suggests large particles *ca*. 200 nm in diameter and this value increases to *ca*. 300 nm at 200 K. The diameters are still small compared to the wavelength of IR light but ($d \approx \lambda / 4\pi \approx 250$ nm) is a more realistic estimate of where effects begin to be significant and Mie scattering theory suggests this is sufficient to produce a slightly asymmetric band profile that skews the centre of gravity to a lower wavenumber while having less effect on the peak maximum position. The MD simulations do not suffer from the Mie scattering derived band shape asymmetry also show a linear blue-shift in COG band position.

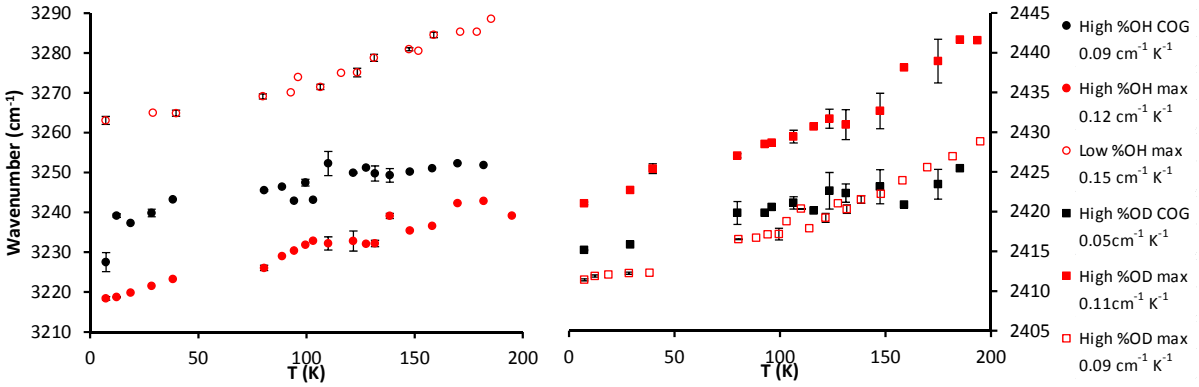

Figure 8: Comparison of the COG band position to the peak max position for the H_2O and D_2O stretching bands as a function of increasing temperature. Max and COG refer to the method used to calculate the peak position, whereas high OH (OD) refers to almost pure H_2O (D_2O) crystalline ice.

Dilute oscillator gradient

The OH stretch, **Figure 6**, is broad with a FWHM of 168 cm^{-1} in pure H_2O. As % OH decreases and the OH oscillators are diluted, the band structure collapses to a single peak with a FWHM of 50 cm^{-1}. At 8 % OH, very little H_2O is present and the OH oscillators that remain are predominantly found in the HOD species. Similarly, HOD is responsible for most of the OD oscillators at low OD concentrations. When HOD is diluted this way, the OH (or OD) oscillators in the absence of inter- and intramolecular coupling can be regarded as a "basis function" or local mode, the intrinsic starting point for building up the phonon modes. Their band positions represent in a straightforward manner the potential energy relation of the OH (or OD) group in the hydrogen bonded environment.

Figure 8 also incorporates the temperature dependence of the dilute OH/OD oscillator bands of HOD. The gradients for dilute OH and OD are 0.15 and 0.09 cm^{-1} K^{-1} respectively. It is significant that the gradients are similar to that of the peak maximum ($W(H_2O)$ or $W(D_2O)$) in the isotopically pure species and are consistent with previous thin film studies of dilute HOD in D_2O [69]. Slight differences between the isolated and H-bonded stretching gradients are mainly due to differences in the intensities of the bands. The dilute oscillator bands have intensities much weaker than their H-bonded counterparts and consequently the real refractive index values in that region of the spectrum are less affected, the scattering related band shape changes and shifts are greatly diminished. In turn this will give a slightly different gradient. From these results, it is possible to conclude and confirm that the blue-shift with increasing temperature observed in crystalline ice is almost entirely due to the intrinsic change in the local hydride potential energy as H-bonding is weakened, rather than to any consequent changes in intermolecular coupling between oscillators.

Dangling OH

The "free" or "dangling" OH band (dOH) around 3693 cm^{-1} does not shift over the temperature range from 80 - 170 K, as shown in **Figure S3** in the supplementary data. Between 40 - 70 K, the dOH band is red-shifted due to the onset of nitrogen adsorption onto the aerosol surface. The associated OH--N_2 vibrational mode is observed at a wavenumber value of 3670 cm^{-1} which is consistent with previous studies [12, 70].

The temperature range observed here is slightly higher than in the study by Hujo *et al*. [71], where the onset of N_2 adsorption began at 30 K for small clusters of 100 water molecules (1.8 nm diameter). This discrepancy in temperature is most likely due to the partial pressure of N_2 or to the dependence on cluster size. The relative proportion of N_2 molecules to available dOH sites has an appreciable influence on the temperature for N_2 adsorption. This is evidenced by the elevated temperature of 120 K found in experiments that used a substantial N_2 pressure of 0.4 bar [see **Figure 1** in [70]) in comparison to < 0.1 mbar in the study by Hujo *et al* [71]. The concentration of N_2 in this study is most likely higher than that used in [71]. Particle size may also be a factor, as those measured by Hujo et al were at least two times smaller than the particles observed in this study even at the coldest temperatures. Cluster size influences the intrinsic position of the dOH band, which has a position of 3692 cm^{-1} for large particles in comparison to > 3700 cm^{-1} for small particles [46] and is indicative of more strongly H-bonded H_2O molecules and more polarised dOH bonds. This would lead to stronger OH…N_2 interactions for larger clusters, and hence adsorption could occur at a higher temperature.

OH/OD stretching modes vs concentration

The experimental results of isotopic variation in the OH and OD stretch regions are shown in **Figure 9**. The local OH oscillator band of dilute HOD in D_2O is narrow with a simple lineshape. This broadens initially with more HOD present and then as the H ratio increases still, the triple peak band contour associated with H_2O gradually emerges. It is much broader overall, and red-shifted. These trends are well reproduced in the corresponding simulations shown in **Figure 10**, though it is noticeable that the corresponding simulations have greater FWHM linewidths (e.g. 50 cm^{-1} for dilute OD and 75 cm^{-1} for dilute OH). From the 2nd derivative analysis, the absolute positions and the relative distance

between the SH and W peaks in the OH stretching region remains consistent across the dilution range where they are observable (*ca*. 37 – 100 %), with a separation of *ca*. 140 cm^{-1}. In contrast to the SH band, the SL phonon band is red-shifted from its first observable position when OH < 50 % (3149 cm^{-1} at 47 %) to 3126 cm^{-1} at 97 % OH.

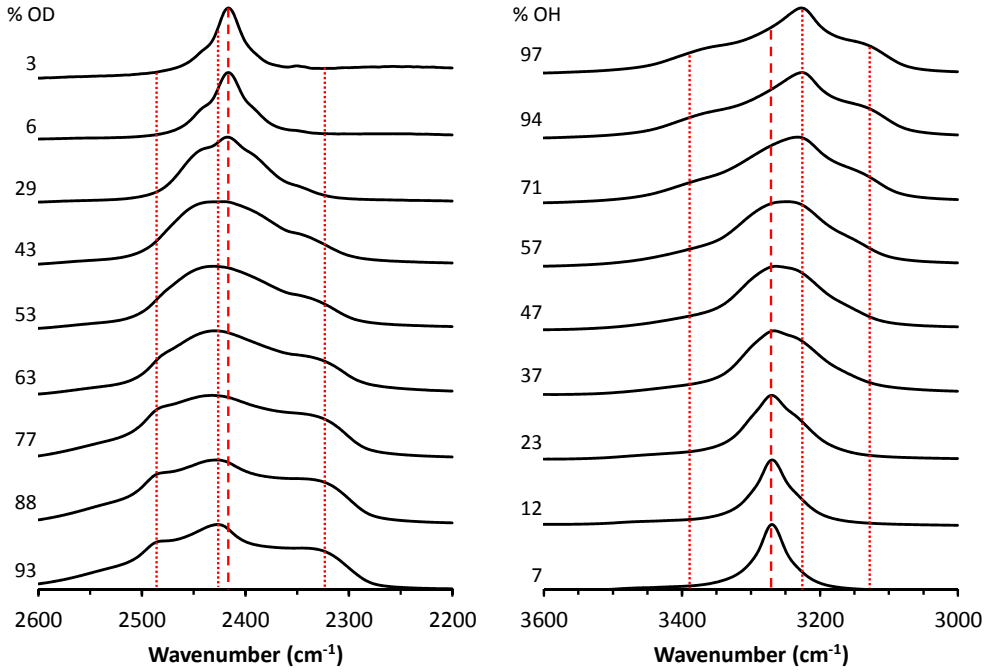

Figure 9: Changes in the OD (left) and OH(right) hydride bands at 78 K as a function of % OD and % OH respectively. The dotted lines represent peaks 2, 3 and 4 of the H-bonded band, whereas the dashed lines show the position of the ν_1 and ν_3 bands of HOD respectively.

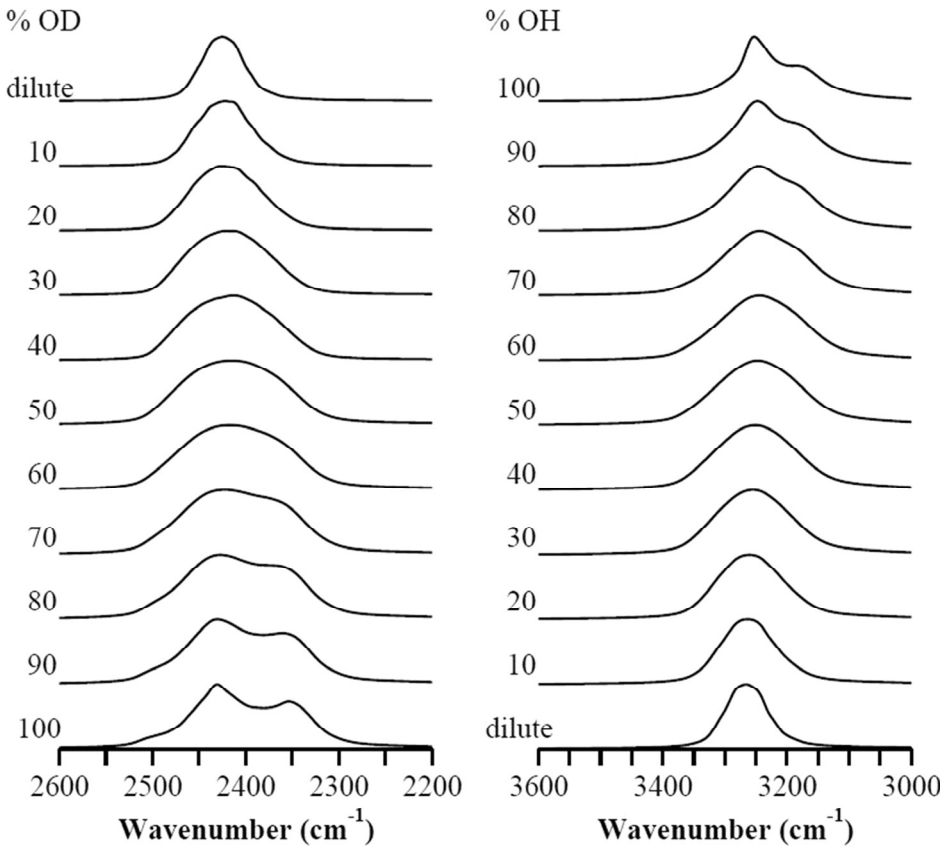

Figure 10: Calculated OD and OH stretching bands at 78 K as a function of % OD and % OH respectively.

The band shifts that take place as OH (or OD) oscillator concentration increases are also instructive. In the OH stretch region, the COG wavenumber value is red-shifted in a linear manner from 3270 to 3240 cm^{-1} (**panel a** in **Figure 11**), while the corresponding peak maximum shifts from 3270 to 3226 cm^{-1}. The MD simulations provide a very similar result, with a linear reduction in COG band position (open circles in **Figure 11**) together with a red-shift in the peak 3 maximum of 15 cm^{-1}.

In the OD stretch region, even at OD concentrations as low as 6 %, shoulder bands are evident at *ca*. 2440 and 2380 cm^{-1} (see **Figure 9** in text and **Figure 3** in [15]). The D_2O concentration should still be negligible and the spectral features must arise entirely from OD oscillators in HOD molecules largely surrounded by H_2O. The intensity of the high wavenumber shoulder band gradually increases with increasing % OD, and its position exhibits a modest blue-shift when % OD is increased from 2.7 % to 30 % (2445 to 2450 cm^{-1}). Beyond this point, the proportion of OD is high enough that D_2O concentration becomes significant and the spectrum smears out before the phonon features associated with the D_2O profile evolve. The low wavenumber shoulder band position shows a similar trend. Similar early hints of sub-band structure are observed in the OH spectra with the appearance of a high wavenumber shoulder at 10 – 30 % OH. The appearance of phonon like band structure even with quite dilute OD (and OH) oscillators implies strong intermolecular coupling and a high degree of delocalisation, as shown in previous theoretical studies [58, 60]. Broadening of the W peak in both H-bonded OH and OD scenarios, as % OH (% OD) is increased further, may be due to increased inter- and intramolecular coupling.

The OD stretch bands, surprisingly, show two different trends for the COG band position as shown in **panel b** in **Figure 11**. Firstly, as % OD increases toward 60 %, the COG average wavenumber value is red-shifted. Although the peak maximum broadens and shifts to higher wavenumber, a low wavenumber phonon band at *ca*. 2330 cm^{-1} becomes evident at 30 % OD. It shifts slightly to 2319 cm^{-1} and becomes prominent at 50 % OD where HOD is still the dominant species, but then does not shift any further with increasing % OD. This sub-band is also evident in the corresponding MD simulations (**Figure 10**). Its early evolution suggests highly delocalized vibrational eigenstates due to both strong intramolecular and intermolecular couplings that are in a sense "saturated" already at *ca*. 50 % (theoretically, this could be framed as a percolation threshold).

However, with further increases in OD concentration beyond 60 %, the overall band system is then blue-shifted to the extent that at 92 % OD the COG position of 2420 cm^{-1} is higher than in the low OD limit. This trend is opposite to that observed in the OH stretch region. The spectra in **Figure 9** reveal the growth of a shoulder band at *ca*. 2480 - 2490 cm^{-1}, along with an increasingly pronounced high wavenumber tail to the band profile. In the MD simulations, neither of these features is very well reproduced and even at higher % OD concentrations the COG average band position is increasingly red-shifted (**panel b** in **Figure 11**). These observations raise the question of whether the omission of Fermi resonance interactions with the $2\nu_2$ band overtone level in D_2O may be responsible for the discrepancy.

The expected position of the $2\nu_2$ band is affected by the difficulty in pinning down the ν_2 band fundamental for bulk crystalline ice. A value of 1735 cm^{-1} has been found for H_2O isolated in D_2O at 90 K [86], while *ab initio* results and extrapolation of bend vs stretch mode wavenumber values as H-bond strength changes suggest a value closer to 1708 cm^{-1} [11]. The ν_2 fundamental of D_2O isolated in H_2O has also been measured at 1225 cm^{-1} [18] but subsequently estimated to be closer to 1265 cm^{-1} [86]. HOD diluted in D_2O or H_2O is observed at 1510 or 1490 cm^{-1} respectively. Anharmonic constants $2X_{22}$ = - 38 cm^{-1} for H_2O, - 25 cm^{-1} for HOD and - 20 cm^{-1} for D_2O may be obtained from well determined gas phase monomer values for the ν_2 and $2\nu_2$ bands [29, 36, 87]. Using these values the $2\nu_2$ band positions in crystalline ice may be estimated as 3378 - 3432 cm^{-1} for H_2O, 2930 - 2970 cm^{-1} for HOD and 2430 - 2510 cm^{-1} for D_2O. This puts the $2\nu_2$ band of HOD quite some distance from the hydride stretches, while for the other two isotopologues, this same band is a little higher than the associated hydride stretch band centres. In D_2O the spacing is very close and therefore more likely to influence the underlying band structure on the high wavenumber side and is consistent with our observations. Rice *et al*. [90] included this Fermi resonance in modelling of the IR and Raman band profiles, concluding that it significantly improved the simulations in the D_2O case. Even so, the IR simulations did not reproduce the shoulder and tail seen on the high wavenumber side of the experimental spectra. It is entirely possible that the value used for the ν_2 fundamental in that modelling (1220 cm^{-1}) is too low and that a value closer to 1265 cm^{-1} [86] might be required.

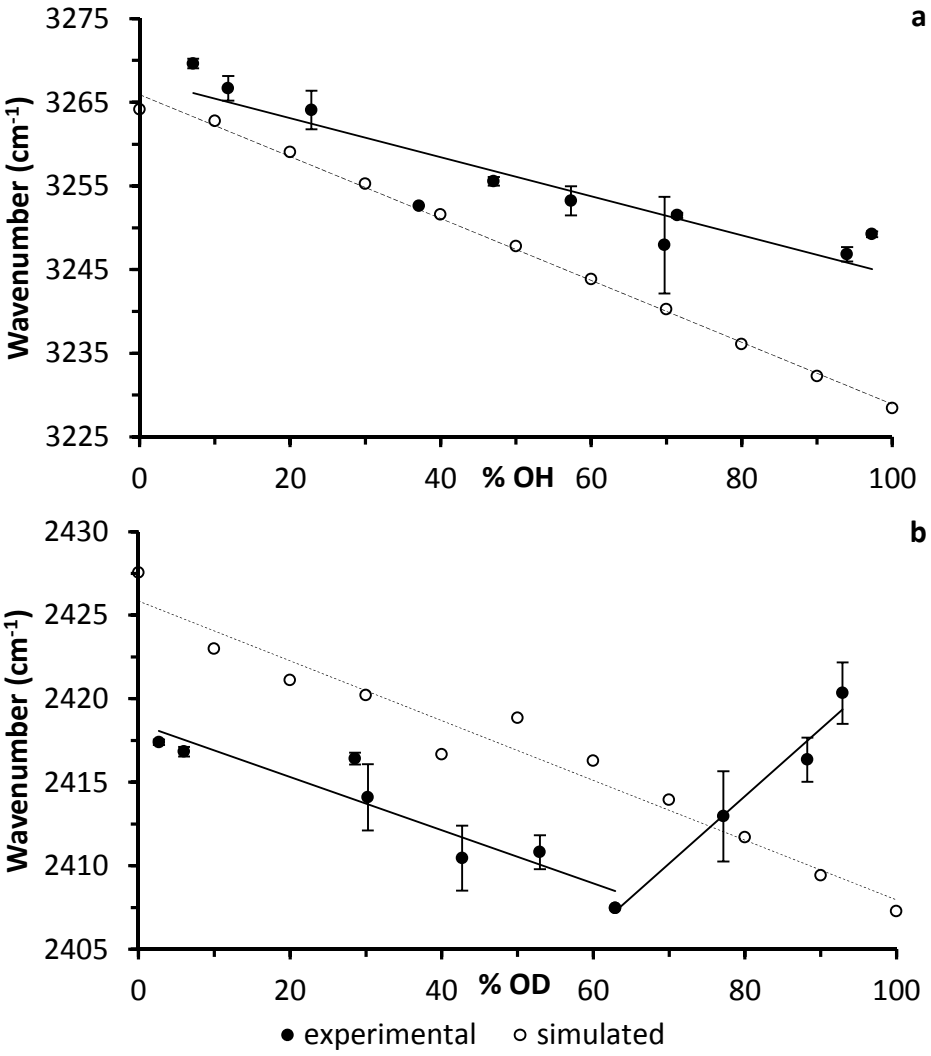

Figure 11: Wavenumber shifts for the H-bonded OH (**panel a**) and OD (**panel b**) stretching bands at 78 K as a function of increasing % OH respectively.

The FWHM of the band profiles in the OH and OD stretch regions are comparable across the entire dilution range (**Figure S4** in the supplementary data) and even the FWHM of the dilute (HOD) peaks are the same in the OH and OD regions. This is unexpected as crystalline D_2O produces more linear H-bonds, compared to H_2O [91], which should lead to narrower band widths for each sub-band. The reduced mass of the OD oscillators should also decrease the magnitude of the couplings and therefore reduce the distances between sub-bands. This narrowing is supported by the frequency distribution calculations performed by Shi *et al*. (**Figure 14** in [58]), where the frequency distributions for the weak intermolecular phonon modes in D_2O are calculated to be approximately 25 % less than H_2O. The decrease in FWHM for the OH stretch beyond 94 % OH is simply due to the increased height of narrow central peak 3.

Dangling OH/OD bands

The dangling OH and OD bands associated with the particle surface also show some changes with isotopic concentration, as seen in **Figure 12**. As the concentration of OD is increased, the dangling OH band for H_2O at 78 K is slightly blue-shifted from 3693 to 3696 cm^{-1}. The band is also broadened and appears as an unresolved doublet with a second, more intense peak becoming visible near 3688 cm^{-1} at 13 % OH (top trace in the left panel of **Figure 12**). A similar observation was made by Rowland *et al*. [70] for microporous amorphous ice particles, where the singlet dangling band changed to a broad, unresolved feature and the dangling bands for surface OH groups from H_2O and HOD were observed at 3692 and 3686 cm^{-1} respectively at 80 K. It is known that the surface layers of ice aerosols are quite disordered (e.g. amorphous H_2O bending feature near 1649 cm^{-1}) and so it is not surprising that the observed position for the dangling OH groups are similar to those of amorphous ice. These dangling bands are assigned to 3 co-ordinate water molecules (double H-bond acceptor, single donor). There is little evidence for 2 co-ordinate (single donor, single acceptor) molecules in our spectra, which exhibit signature bands around 3720 cm^{-1} in both microporous amorphous ice particles [70] and in small gas phase clusters [92].

In the case of the dangling OD groups, the two bands are more resolved and have larger splitting of *ca*. 14 cm^{-1}. The dangling OD group from HOD is observed at a lower wavenumber (2712 cm^{-1}) compared to D_2O (2726 cm^{-1}). Beyond 43 % OH, the intensity of the dangling OD bands was too weak to be observed, probably due to the preference for single donor HOD molecules on the surface to be deuterium bonded [28]. These assignments and shifts are supported by harmonic frequency calculations at the CCSD(T)/CBS level on isotopologues of the water dimer [93]. In the dimer, the dangling OH stretch of a HOD donor molecule is 8 cm^{-1} lower than a corresponding H_2O donor, while the dangling OD stretch of HOD is red-shifted 14 cm^{-1} compared to D_2O. The agreement with the aerosol data suggests that these shifts are due to intramolecular coupling that is greater in D_2O than in H_2O.

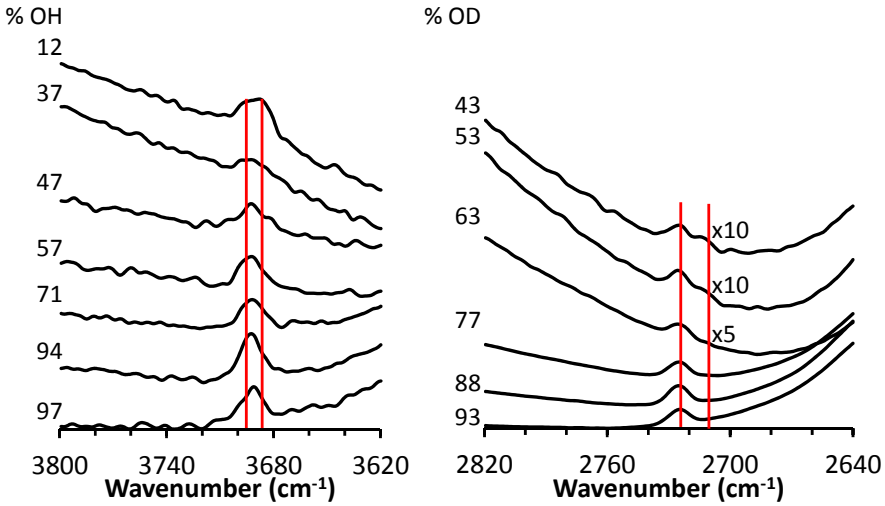

Figure 12: Changes in the dangling OH (left) and OD (right) bands at 78 K as the concentration of OH and OD are increased.

Conclusions

The mid-IR spectra of nanoparticle ices have been recorded over a range of temperatures as well as at different isotopic concentrations. Analysis of the spectra has allowed us to address how the effects of particle size, temperature and isotopic dilution influence the observed spectra, as well as the interplay between intermolecular and intramolecular coupling within the ice lattice.

Particle size affects the spectra of all three isotopologues, at the small size limit (diameters near *ca* 10 - 20 nm) due to substantial contribution from amorphous surface layers and at the large limit (300 nm) due to scattering. However, the degree of influence differs greatly depending on the vibrational band. For the ν_L libration bands, the observed red-shift with temperature is modest in magnitude, and the band position may be significantly red-shifted by either small or large particle effects. The significance of this is to confirm our recent findings that the ν_L libration band is not a useful for estimating temperature profiles in clouds [12]. The analyses suggest that the OH stretching band is a far better marker for estimating cloud temperature.

Within the bending region of H_2O, D_2O and HOD, all three exhibit quite different behaviours. We assign the dominant broad feature centred at 1580 $cm^{-`}$ in spectra at 80 K to the $2\nu_L$ band following the results presented by Devlin and co-workers [11, 86]. The narrower band around 1650 cm^{-1}, enhanced at temperatures over 140 K, and most intense for small particles, is assigned to ν_2 vibrations of more amorphous, disordered molecules found on the surface layers or at high temperatures. The $2\nu_L$ band in near pure crystalline D_2O ice is asymmetrical in shape with a peak max at 1211 cm^{-1} at 78 K, and is insensitive to both temperature and particle size. A notional spectrum of the ν_2(HOD) band has also been derived by subtracting off spectral features emanating from both parent isotopologues. The width of this band, located near 1500 cm^{-1}, is relatively small (half-width half-max of *ca*. 70 cm^{-1} compared to *ca*. 320 cm^{-1} and 145 cm^{-1} for the $2\nu_L$ bands of H_2O and D_2O) suggesting that it may be primarily ν_2 in nature. The nature of the spectra in this region and the reasons for the significant isotopic differences remain unclear. The different libration motions and the likelihood of $\nu_2/2\nu_L$ Fermi resonance makes for a complex analysis and these bands are yet to benefit from the same level of scrutiny by theoretical methods as the hydride stretches have received.

As isotopic dilution is varied, the broad $\nu_L(H_2O)$ band decreases in width (and intensity) and is red-shifted to the corresponding value for dilute HOD in D_2O. The $2\nu_L(D_2O)$ band is barely blue-shifted as % OD is changed from near 0 to almost 100 %. A feature for the ν_2(HOD) band becomes prominent at approximately equal proportions of OH and OD, and is seen on the ”red shoulder” of the $2\nu_L(H_2O)$ band. The position of this band varies depending on the host matrix due to Fermi resonance (1487 cm^{-1} in mostly H_2O and to 1508 cm^{-1} in mostly D_2O at 78 K). The intensity of the $2\nu_L(H_2O)$ band decreases with increasing % OD and is replaced with the $3\nu_L(D_2O)$ band around 1632 cm^{-1} at 93 % OD.

Several different trends are observed for the hydride stretching bands which are dependent on the method used to determine the band position. At least three sub-components are evident in the case of near pure H_2O and D_2O. The peak maximum for the overall band system, corresponding to the most intense central peak, when plotted against temperature shows a positive linear trend, and similar gradients are found for the high and low wavenumber shoulder peaks evaluated using

second derivatives. At higher temperatures, the particles generated are large enough (*ca.* 300 nm) for scattering to begin to influence the central peak maxima to a small extent, but the COG position for the band system as a whole changes to a greater extent such that a net red-shift is observed. The band shapes of the dilute OH/OD oscillators for HOD in H_2O or D_2O are much less influenced by scattering due to their lack of intensity, since low values of the imaginary refractive indices (*k*) in that region correspond to only small local deviations of the real refractive indices (*n*). The blue-shift gradients for the isolated OH (or OD) oscillators are very similar (*ca*. 25 % more (for OH) and 20 % less (for OD)) than the corresponding peak maxima for near pure H_2O and D_2O ices. This supports the argument that the blue-shift in the hydride band position with temperature is predominantly due to the intrinsic change in the local OH (or OD) oscillator potential, and that weakening of intermolecular coupling of OH (or OD) oscillators has little influence.

Dramatic changes in the OH and OD stretch band profiles with increasing isotopic oscillator concentration clearly illustrate the high degree of delocalisation in the vibrations of neat ices. Furthermore, two different trends are observed for the COG peak position of the OH and OD stretches. The OH stretch band is linearly red-shifted as % OH changes from near 0 % (corresponding to dilute HOD in D_2O) and approaches 100 % (corresponding to pure H_2O). In contrast to the OH stretch, the OD stretch band shows a red-shift as % OD changes from near 0 % to 60 %. Beyond this point, the OD stretch band is blue-shifted such that the position of the OD stretch in near pure D_2O is at a higher wavenumber value than the OD stretch of dilute HOD in H_2O. This highlights the effect of Fermi resonance in this region, albeit its influence is much more significant in D_2O than H_2O due to closer proximity of the $2\nu_2$ level. Although the COG positions of both bands changes as a function of isotopic concentration, the positions of the intermolecular W peaks (in both OD and OD stretching bands) only change by a few wavenumbers with isotopic dilution and this is indicative of the delocalised nature of the stretching bands.

It is notable that the MD simulations which do not account for the Fermi resonance can reproduce well the triple peak structure of crystalline H_2O, its blue-shift with temperature and the red-shift in band position with increasing OH oscillator concentration. The same calculations do not perform so well in the OD region and the simulated contours at high D_2O concentration show a lack of intensity in the high wavenumber shoulder and the overall red-shifted band position (as in the OH case) in contrast to experiment.

In the case of the dangling OH and OD groups, it has been possible to experimentally resolve the separate contributions that arise depending on whether the H-bonded atom is H or D, and the splitting is larger in the OD region (*ca*. 14 cm^{-1}) than in the OH region (*ca*. 8 cm^{-1}).

Being able to accurately determine the positions of the $\nu_2(H_2O)$ and $\nu_2(D_2O)$ bands remains a challenge as both are intrinsically weak in crystalline ices and there is large overlap with the $2\nu_L(H_2O)$ and $3\nu_L(D_2O)$ bands in the case of H_2O. This affects the estimation of the $2\nu_2$ band position which is important for determining the magnitude of Fermi resonance between ν_1 and $2\nu_2$ in D_2O, subsequently affecting the band shape of the simulated spectra as pointed out by Hernandez *et al*. [86]. Although some aspects of this research require further clarification, we have been able to identify the underlying causes for changes in band shapes (due to particle size and isotopic dilution) and band positions (due to Fermi resonance, isotopic dilution, temperature and changes in oscillator strength) that were observed in our experimental spectra.

Acknowledgements

We gratefully acknowledge the Australian Synchrotron and thank the staff for their assistance with experiments at the Far-IR beamline. AW thanks the Monash University Faculty of Science for a Dean's postgraduate scholarship, and RA is grateful for a La Trobe University Postgraduate Scholarship. We appreciate the insightful discussions with Prof. James. L. Skinner.

References

[1] A. Falenty, T. C. Hansen and W. F. Kuhs, *Nature*, **516**, 231 (2014).
[2] J. B. Hasted, S. K. Husain, F. A. M. Frescura and J. R. Birch, *Chem. Phys. Lett.*, **118**, 622 (1985).
[3] C. Medcraft, D. McNaughton, C. D. Thompson, D. Appadoo, S. Bauerecker and E. G. Robertson, *Astrophys. J.*, **758**, 17 (2012).
[4] J. E. Bertie, *Appl. Spectrosc.*, **22**, 634 (1968).
[5] J. E. Bertie and E. Whalley, *J. Chem. Phys.*, **46**, 1271 (1967).
[6] L. Shi, Y. Ni, S. E. P. Drews and J. L. Skinner, *J. Chem. Phys.*, **141**, 084508 (2014).
[7] V. Buch and J. P. Devlin, *J. Chem. Phys.*, **94**, 4091 (1991).
[8] F. Montmessin, F. Forget, P. Rannow, M. Cabane and R. M. Haberle, *J. Geophys. Res.*, **109**, E10004 (2004).
[9] D. C. B. Whittet, R. G. Smith, A. J. Adamson, D. K. Aitken, J. E. Chiar, T. H. Kerr, P. F. Roche, C. H. Smith and C. M. Wright, *Astrophys. J.*, **458**, 363 (1996).
[10] J. P. Devlin, *J. Chem. Phys.*, **91**, 5850 (1989).
[11] J. P. Devlin, J. Sadlej and V. Buch, *J. Phys. Chem. A*, **105**, 974 (2001).
[12] C. Medcraft, D. McNaughton, C. D. Thompson, D. R. T. Appadoo, S. Bauerecker and E. G. Robertson, *Phys. Chem. Chem. Phys.*, **15**, 3630 (2013).
[13] R. M. Mastrapa, S. A. Sandford, T. L. Roush, D. P. Cruikshank and C. M. D. Ore, *Astrophys. J.*, **701**, 1347 (2009).
[14] M. W. Severson, J. P. Devlin and V. Buch, *J. Chem Phys.*, **119**, 4449 (2003).
[15] C. Haas and D. F. Hornig, *J. Chem. Phys.*, **32**, 1763 (1960).
[16] J. E. Bertie and S. M. Jacobs, *J. Chem. Phys.*, **67**, 2445 (1977).
[17] P. A. Giguére and K. B. Harvey, *Can. J. Chem.*, **34**, 798 (1956).
[18] J. P. Devlin, P. J. Wooldridge and G. Ritzhaupt, *J. Chem. Phys.*, **84**, 6095 (1986).
[19] M. N. Afsar and J. B. Hasted, *J. Opt. Soc. Am.*, **67**, 902 (1977).
[20] J. –J. Max and C. Chapados, *J. Chem. Phys.*, **116**, 4626 (2002).
[21] Y. Maréchal, *J. Chem. Phys.*, **95**, 5565 (1991).
[22] G. Herzberg, *Molecular Spectra and Molecular Structure*, 281 (1945) Van Nostrand.
[23] J. P. Devlin, C. Joyce and V. Buch, *J. Phys. Chem. A*, **104**, 1974 (2000).
[24] M. S. Bergren, D. Schuh, M. G. Sceats and S. A. Rice, *J. Chem. Phys.*, **69**, 3477 (1978).
[25] J. E. Bertie and E. Whalley, *J. Chem. Phys.*, **40**, 1646 (1964).
[26] F. Perakis, S. Widmer and P. Hamm, *J. Chem. Phys.*, **134**, 204505 (2011).
[27] E. C. W. Clarke and D. N. Glew, *Can .J Chem.*, **50**, 1655 (1972).
[28] J. P. Devlin, *J. Chem. Phys.*, **112**, 5527 (2000).
[29] R. A. Toth, *J. Mol. Spectrosc.*, **195**, 73 (1999).
[30] B. Rowland, N. S. Kadagathur, J. P. Devlin, V. Buch, T. Feldman and M. J. Wojcik, *J. Chem. Phys.*, **102**, 8328 (1995).
[31] A. Shalit, F. Perakis and P. Hamm, *J. Phys. Chem. B*, **117**, 15512 (2013).
[32] A. B. Horn, M. A. Chesters, M. R. S. McCoustra and J. R. Sodeau, *J. Chem. Soc. Faraday Trans.*, **88**, 1077 (1992).
[33] M. A. Everest and C. J. Pursell, *J. Chem. Phys.*, **115**, 9843 (2001).
[34] A. Millo, Y. Raichlin and A. Katzir, *Appl. Spectrosc.*, **59**, 460 (2005).
[35] S. Y. Venyaminov and F. G. Prendergast, *Anal. Biochem.*, **248**, 234 (1997).
[36] R. A. Toth, *J. Mol. Spectrosc.*, **195**, 98 (1999).
[37] C. Medcraft, E. G. Robertson, C. D. Thompson, S. Bauerecker and D. McNaughton, *Phys. Chem. Chem. Phys.*, **11**, 7848 (2009).
[38] J. P. Devlin, C. A. Yinnon and V. Buch, *Phys. Chem. Chem. Phys.*, **11**, 7819 (2009).
[39] Ó. F. Sigurbjörnsson, G. Firanescu and R. Signorell, *Phys. Chem. Chem. Phys.*, **11**, 187 (2009).
[40] T. Häber, U. Schmitt and M. A. Suhm, *Phys. Chem. Chem. Phys.*, **1**, 5573 (1999).
[41] R. Signorell, M. K. Kunzmann and M. A. Suhm, *Chem. Phys. Lett.*, **329**, 52 (2000).
[42] M. Jetzki and R. Signorell, *J. Chem. Phys.*, **117**, 8063 (2002).

[43] R. Signorell and D. Luckhaus, *J. Phys. Chem. A*, **106**, 4855 (2002).
[44] M. Seaver, A. Galloway and T. J. Manuccia, *Rev. Sci. Instrum.*, **60**, 3452 (1989).
[45] E. J. Davis, *Aerosol Sci. Tech.*, **26**, 212 (1997).
[46] V. Buch, S. Bauerecker, J. P. Devlin, U. Buck and J. K. Kazimirski, *Int. Rev. Phys. Chem.*, **23**, 375 (2004).
[47] G. Firanescu, D. Hermsdorf, R. Ueberschaer and R. Signorell, *Phys. Chem. Chem. Phys.*, **8**, 4149 (2006).
[48] C. D. –Grau and D. Marx, *Phys. Rev. Lett.*, **112**, 148302 (2014).
[49] C. Q. Sun, X. Zhang, X. Fu, W. Zheng, J. –L. Juo, Y. Zhou, Z. Shen and J. Zhou, *J. Phys. Chem. Lett.*, **4**, 3238 (2013).
[50] M. Praprotnik, D. Janežič and J. Mavri, *J. Phys. Chem. A.*, **108**, 11056 (2004).
[51] M. J. Wójcik, K. Szczeponek and S. Ikeda, *J. Chem. Phys.*, **117**, 9850 (2002).
[52] S. Imoto, S. S. Xantheas and S. Saito, *J. Chem. Phys.*, **138**, 054506 (2013).
[53] Y. Huang, X. Zhang, Z. Ma, Y. Zhou, W. Zheng, J. Zhou and C. Q. Sun, *Coord. Chem. Rev.*, **285**, 109 (2015).
[54] Y. Huang, Z. Ma, X. Zhang, G. Zhou, Y. Zhou and C. Q. Sun, *J. Phys. Chem. B.*, **117**, 13639 (2013).
[55] B. Auer, R. Kumar, J. R. Schmidt and J. L. Skinner, *P. Natl. Acad. Sci. USA*. **104**, 14215 (2007).
[56] C. P. Lawrence and J. L. Skinner, *J. Chem. Phys.*, **118**, 264 (2003).
[57] S. A. Corcelli and J. L. Skinner, *J. Phys. Chem. A*, **109**, 6154 (2005).
[58] L. Shi, S. M. Gruenbaum and J. L. Skinner, *J. Phys. Chem. B*, **116**, 13821 (2012).
[59] F. Li and J. L. Skinner, *J. Chem. Phys.*, **132**, 204505 (2010).
[60] F. Li and J. L. Skinner, *J. Chem. Phys.*, **133**, 244504 (2010).
[61] L. Shi, F. Li and J. L. Skinner, *J. Chem. Phys.*, **140**, 244503 (2014).
[62] L. Shi and J. L. Skinner, *J. Chem. Phys.*, **143**, 014503 (2015).
[63] C. J. Tainter, L. Shi and J. L. Skinner, *J. Chem. Phys.*, **140**, 134503 (2014).
[64] J. Ceponkus and B. Nelander, *J. Phys. Chem. A*, **108**, 6499 (2004).
[65] M. E. Fajardo, S. Tam and M. E. DeRose, *J. Mol. Struct.*, **695-696**, 111 (2004).
[66] G. Ritzhaupt and J. P. Devlin, *J. Chem. Phys.*, **67**, 4779 (1977).
[67] E. A. Raymond, T. L. Tarbuck, M. G. Brown and G. L. Richmond, *J. Phys. Chem. B*, **107**, 546 (2003).
[68] Z. Wang, A. Pakoulev, Yonsoo Pang and D. D. Dlott, *J. Phys. Chem. A*, **108**, 9054 (2004).
[69] T. A. Ford and M. Falk, *Can. J. Chem.*, **46**, 3579 (1968).
[70] B. Rowland, M. Fisher and J. P. Devlin, *J. Chem. Phys.*, **95**, 1378 (1991).
[71] W. Hujo, M. Gaus, M. Schultze, T. Kobař, J. Grunenberg, M. Elstner and S. Bauerecker, *J. Phys. Chem. A*, **115**, 6218 (2011).
[72] S. Bauerecker, M. Taraschewski, C. Weitkamp, H. K. Cammenga, *Rev. Sci. Instrum.*, **72**, 3946 (2001).
[73] J. L. Skinner, B. M. Auer and Y. –S. Lin, *Advances in Chemical Physics*, *Volume 142* , edited by Stuart A. Rice Copyright © 2009 John Wiley & Sons, Inc.
[74] V. Buch, R. Martoňák and M. Parrinello, *J. Chem. Phys.*, **123**, 051108 (2005).
[75] L. G. Dowell and A. P. Rinfret, *Nature*, **188**, 1144 (1960).
[76] V. F. Petrenko and R. W. Whitworth, *Physics of Ice*, Oxford University Press, Oxford 1999.
[77] C. J. Tainter, P. A. Pieniazek, Y. –S. Lin and J. L. Skinner, *J. Chem. Phys.*, **134**, 184501 (2011).
[78] B. Hess, C. Kutzner, D. v. d. Spoel and E. Lindahl, *J. Chem. Theory Comput.*, **4**, 435 (2008).
[79] D. M. Hudgins, S. A. Sandford, L. J. Allamandola and A. G. G. M. Tielens, *Astrophys. J. Suppl. S.*, **86**, 713 (1993).
[80] S. Bauerecker, A. Wargenau, M. Schultze, T. Kessler, R. Tuckermann and J. Reichardt, *J. Chem. Phys.*, **126**, 134711 (2007).
[81] L. S. Bartell and J. Huang, *J. Phys. Chem.*, **98**, 7455 (1994).
[82] L. S. Bartell, *J. Phys. Chem.*, **100**, 8197 (1996).

[83] L. Delzeit and D. Blake, *J. Geophys. Res.*, **106**, 33371 (2001).
[84] G. P. Johari, *J. Chem. Phys.*, **122**, 194504 (2005).
[85] M. L. Clapp, R. E. Miller and D. R. Worsnop, *J. Phys. Chem.*, **99**, 6317 (1995).
[86] J. Hernandez, N. Uras and J. P. Devlin, *J. Chem. Phys.*, **108**, 4525 (1998).
[87] V. Buch and J. P. Devlin, *J. Chem. Phys.*, **110**, 3437 (1999).
[88] R. Feistel and W. Wagner, *J. Phys. Chem. Ref. Data*, **35**, 1021 (2006).
[89] T. Salmi, V. Hänninen, A. L. Garden, H. G. Kjaergaard, J. Tennyson and L. Halonen, *J. Phys. Chem. A*, **112**, 6305 (2008).
[90] S. A. Rice, M. S. Bergren, A. C. Belch and G. Nielson, *J. Phys. Chem.*, **87**, 4295 (1983).
[91] M. H. Brooker, G. Hancock, B. C. Rice and J. Shapter, *J. Raman Spectrosc.*, **20**, 683 (1989).
[92] E. G. Robertson, *Chem. Phys. Lett.*, **325**, 299 (2000).
[93] R. Kalescky, W. Zou, E. Kraka and D. Cremer, *Aust. J. Chem.*, **67**, 426 (2014).